

Geophysical Research Letters®

RESEARCH LETTER

10.1029/2021GL095537

Key Points:

- A new shape model of small fresh lunar craters with normal, central mound, flat-bottomed, and concentric geometry is constructed
- Degradation effect on morphology of small craters and regolith thickness estimation is studied using a topographic diffusion model
- The small crater morphology method for regolith thickness estimation is revised and applied to the Apollo 11 and 14 landing sites

Supporting Information:

Supporting Information may be found in the online version of this article.

Correspondence to:

W. Fa,
wzfa@pku.edu.cn

Citation:

Yang, X., Fa, W., Du, J., Xie, M., & Liu, T. (2021). Effect of topographic degradation on small lunar craters: Implications for regolith thickness estimation. *Geophysical Research Letters*, 48, e2021GL095537. <https://doi.org/10.1029/2021GL095537>




Received 10 AUG 2021

Accepted 29 OCT 2021

Author Contributions:

Conceptualization: Wenzhe Fa, Minggang Xie
Data curation: Xi Yang
Formal analysis: Xi Yang, Wenzhe Fa, Minggang Xie
Funding acquisition: Wenzhe Fa
Investigation: Xi Yang, Wenzhe Fa, Tiantian Liu
Methodology: Wenzhe Fa, Jun Du, Minggang Xie
Project Administration: Wenzhe Fa
Resources: Wenzhe Fa
Software: Jun Du
Supervision: Wenzhe Fa
Validation: Wenzhe Fa
Writing – original draft: Xi Yang, Wenzhe Fa
Writing – review & editing: Wenzhe Fa, Jun Du, Minggang Xie, Tiantian Liu

Effect of Topographic Degradation on Small Lunar Craters: Implications for Regolith Thickness Estimation

Xi Yang^{1,2}, Wenzhe Fa^{2,3,4} , Jun Du^{2,5}, Minggang Xie⁶ , and Tiantian Liu^{2,7} 

¹Institute of Theoretical and Applied Geophysics, School of Earth and Space Sciences, Peking University, Beijing, China, ²Institute of Remote Sensing and Geographical Information System, School of Earth and Space Sciences, Peking University, Beijing, China, ³State Key Laboratory of Lunar and Planetary Sciences, Macau University of Science and Technology, Macau, China, ⁴Center for Excellence in Comparative Planetology, Chinese Academy of Sciences, Hefei, China, ⁵Now at State Key Laboratory of Space Weather, National Space Science Center, Chinese Academy of Sciences, Beijing, China, ⁶College of Science, Guilin University of Technology, Guilin, China, ⁷Now at Museum für Naturkunde, Leibniz Institute for Evolution and Biodiversity Science, Berlin, Germany

Abstract Small crater morphology method has been used extensively in lunar regolith thickness estimation. However, topographic degradation can change crater morphology and thus bias regolith thickness estimation. In this study, we first developed a shape model for small fresh craters with normal, central mound, flat-bottomed, and concentric geometry. We then simulated their degradation processes by using a topographic diffusion model. Simulation results show that as a small crater degrades, its morphology changes from concentric/central mound to flat-bottomed, from flat-bottomed to normal, and from normal to invisible, depending on its initial morphology. Upon the time a crater becomes invisible, its diameter can be enlarged by a factor of ~70%. We proposed a revised small crater morphology method and applied it to the Apollo 11 and 14 landing sites. Our revised method permits a more accurate estimate of regolith thickness, and our results are helpful in understanding the evolution of the Moon's surface.

Plain Language Summary On the Moon's surface, small impact craters generally exhibit four typical morphologic types: normal, central mound, flat-bottomed, and concentric. Laboratory impact experiments show that morphology of small craters depends primarily on the thickness of the regolith layer. With the high-resolution optical images acquired from recent missions, the small crater morphology method has been used extensively to estimate regolith thickness, which can provide critical information for the evolution of lunar surface. However, topography erosion by subsequent micrometeorite bombardments can change the morphology of impact craters, especially for small ones, preventing an accurate estimation of regolith thickness. In this study, we investigated the degradation effect on lunar regolith thickness estimation using small crater morphology method. We first designed an elevation profile model for small fresh craters with different geometry, and then simulated crater degradation processes by using a topographic diffusion model. These simulations give a quantitative measure on the changes in diameter and morphology of a small crater as it degrades. We further proposed a revised small crater morphology method for lunar regolith thickness estimation and applied it to the Apollo 11 and 14 landing sites, and the results are in good agreement with the estimates from small fresh craters only.

1. Introduction

The continuous impacts of large and small meteoroids with the lunar surface over billions of years have created a global fine-grained regolith layer on the Moon. The nature, structure, stratigraphy, and history of regolith not only preserve key information about the Moon's geology, inner solar system impact flux, and solar wind history, but also are important for future in situ explorations (e.g., Fa & Wieczorek, 2012; McKay et al., 1991; Wilcox et al., 2005). Regolith formation is a self-limiting process and can be divided roughly into two stages. Shortly after a solid surface is formed, there is no or little regolith, and both large and small impacts can excavate bedrock and produce new regolith. As time goes on, regolith becomes thicker, and thus only progressively larger impacts can penetrate through the regolith layer and produce new regolith materials. Small impacts only rework the regolith layer already present at this stage. Depending on whether or not regolith layer can be penetrated through (i.e., regolith thickness), small impacts can produce four typical classes of craters with different morphologies: normal, central mound, flat-bottomed, and concentric (Figure S1 in Supporting Information S1; Gault et al., 1966; Quaide

& Oberbeck, 1968). These four types of small impact craters (< 250 m in diameter, Oberbeck & Quaide, 1967) are widespread on the lunar surface, as evident in high-resolution optical images (Bart et al., 2011; Fa et al., 2014; Gault et al., 1966; Quaide & Oberbeck, 1968), providing a window to see the nature of regolith layer.

Laboratory experiments by impacting a projectile against a loose noncohesive granular layer atop a more coherent substrate suggest that the morphology of small craters depends mainly on thickness of the regolith layer (Gault et al., 1966; Oberbeck & Quaide, 1967). This provides a natural means of measuring regolith thickness by using the morphology of small craters. As the morphology and rim-to-rim diameter (D) of a small crater are identified in optical images, an interval range of regolith thickness (d) can be constrained. A normal crater gives a lower limit of regolith thickness as $d > D/4$, a concentric crater yields an upper limit of $d < D/9$, and a central mound or a flat-bottomed crater constrains the range of regolith thickness as $D/9 < d < D/4$. If a large number of small craters within a geological unit are counted, the cumulative distribution of regolith thickness and its statistical values (e.g., mean and median) can be obtained on the basis of the assumption that the spatial distribution of small craters is uniform. With the high-resolution optical images returned by recent lunar missions, such as the Lunar Reconnaissance Orbiter Camera (LROC) Narrow Angle Camera (NAC) images, the small crater morphology method has been applied extensively for regolith thickness estimation (e.g., Bart et al., 2011; Fa et al., 2014; Yue et al., 2019; Xie et al., 2021).

Because of micrometeorite bombardment and other processes (e.g., seismic shaking, thermal stress weathering), the lunar topography evolves with time, a process named topographic degradation (e.g., Fassett & Thomson, 2014; Soderblom, 1970). In general, topographic degradation can enlarge the diameter of a crater and change its morphology. It is worth noting that such effect becomes more prevalent at smaller crater diameters (Fassett & Thomson, 2014). As a result, when applying the small crater morphology method for regolith thickness estimation, topographic degradation would bias the estimate to a larger inferred thickness value. Soderblom (1970) developed a topographic diffusion model that can quantitatively describe the change of surface elevation with time. A key parameter in this model is the diffusivity, κ , the rate at which topography can spread. With the acquirement of new data and the advances in lunar sciences, this model is recently applied to impact craters within the lunar maria and improved knowledge on the topographic diffusivity of the lunar surface is obtained (e.g., Fassett & Thomson, 2014; Xie et al., 2017). All these make it possible to use the topographic diffusion model to investigate the degradation processes of small craters on the Moon. In this study, we quantify the degradation effect on diameter and morphology of small craters, and we then propose a Monte Carlo method for regolith thickness estimation based on topographic diffusion modeling and the spatial correlation of small craters.

2. Topographic Profile Model of Small Fresh Craters

In this study, we use LROC NAC images for small crater selection and NAC digital terrain models (DTMs) for crater topographic profile extraction. The nominal spatial resolution of NAC images is ~ 0.5 m, which is high enough to identify the morphology of a crater with diameter larger than ~ 10 m. In total, we use 42 NAC optical images and 28 NAC DTMs, and we only focus on small fresh craters in the lunar maria (Figure S2 in Supporting Information S1). The spatial resolution for most NAC DTMs is 2 or 3 m, and one of them has a resolution of 5 m. The absolute elevation accuracy of a NAC DTM is generally less than one pixel spacing of the DTM. For instance, NAC DTM offsets from LOLA profiles have been found to be < 10 m horizontally and < 1 m vertically (Henriksen et al., 2017). However, the degradation of an elevation profile only depends on its relative topographic relief (i.e., slope), therefore the absolute precision of the DTM does not affect our result. The relative precision of a DTM is pretty high (better than 0.1 m, see Figure 7 in Cai & Fa, 2020), allowing an accurate extraction of elevation profile for small craters.

In optical images, a crater is regarded as fresh if it has a sharp rim, a bright halo or ejecta rays, and no/few superposed craters. The morphology of a small crater is identified visually on the basis of its shape and shadow pattern (Fa et al., 2014; Oberbeck & Quaide, 1967): (a) a normal crater has either a conical or spherical segment shape and an arcuate shadow pattern; (b) a central mound crater has a pronounced mound on its floor with an opposite shadow pattern compared to the annular shadow of the crater wall; (c) a flat-bottomed crater has an obviously flat floor with a single annular shadow; (d) a concentric crater has a well-developed central pit with a double annular or ring-shaped arcuate shadow pattern. With these criteria, we conduct an

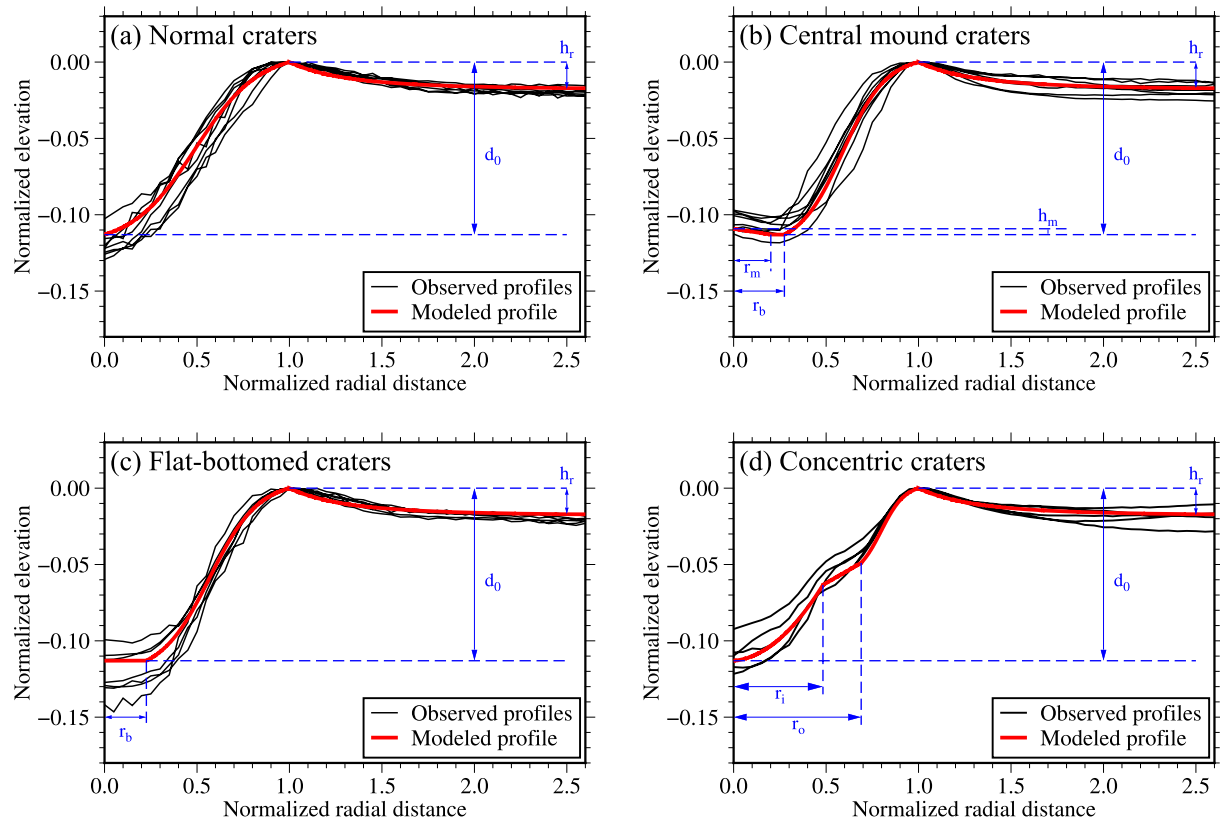


Figure 1. Radial elevation profiles for small fresh craters with different geometry: (a) Normal, (b) Central mound, (c) Flat-bottomed, and (d) Concentric. The elevation is normalized by crater diameter, and the radial distance is normalized by crater radius. The red curves are modeled elevation profiles. d_0 : rim-to-floor depth; h_r : rim height; h_m : mound height; r_m : mound radius; r_b : floor radius; r_i : inner ring radius; r_o : outer ring radius.

exhaustive search for small fresh craters over the lunar mare regions that are covered with both NAC optical images and DTMs (see Figure 1 in Cai & Fa, 2020). We only select craters whose surrounding background topography is relatively flat. In total, 28 small fresh craters with diameters between 36 and 167 m are selected (Figure S2 in Supporting Information S1). Among these craters, eight are normal, eight are central mound, seven are flat-bottomed, and five are concentric craters. For each selected crater, the radial elevation profile is then extracted from NAC DTM data. Background geologic features (e.g., large, nearby craters, and slopes) could result in a large fluctuation in the extracted elevation profile (Du et al., 2019), and hence should be excluded. Therefore, for each crater, only a sector area with the crater center as the vertex is selected in order to exclude atypical terrains (Figure S1 in Supporting Information S1). Furthermore, superposed small craters (if exist) with slopes larger than 10° in the continuous ejecta area are excluded. Finally, the normalized radial elevation profile of each crater is obtained by azimuthally averaging the elevations within the sector (Figure 1).

Recent studies show that morphologies of small lunar craters ($D < 1$ km) are scale-dependent (Mahanti et al., 2018; Stopar et al., 2017; Sun et al., 2018). In order to build up a geometry model for small fresh craters, we first define several diameter-dependent morphometric parameters. Three common morphometric parameters are defined for all types of small craters: crater depth (d_0), rim height (h_r), and decay constant (α , a measure on how elevation decays with distance beyond crater rim). Several other morphometric parameters are further used: floor radius (r_b) for flat-bottomed craters, mound height (h_m), mound radius (r_m), and floor radius (r_b) for central mound craters, and inner ring radius (r_i) and outer ring radius (r_o) for concentric craters. Definitions of these morphometric parameters are illustrated in Figure 1 (blue lines). With the normalized topographic profiles of fresh craters, we then derive the diameter dependence of these morphometric parameters by using a power law or a linear relationship between each parameter and diameter (Figures S3–S7 in Supporting Information S1). In the fitting of the morphometric parameters using a power law function, all the R^2 values are

Table 1
Mathematic Expressions for the Shape of Small Fresh Impact Craters on the Lunar Mare

Morphology	Diameter range (m)	Elevation profile	Parameters
Normal	$40 < D < 100$	$h(r) = \begin{cases} C \frac{\exp(br) - \exp(b)}{1 + \exp(a + br)}, & r \leq 1 \\ h_r(r^\alpha - 1), & 1 < r \leq 2.5 \end{cases}$	$a = -2.8567$ $b = 5.8270$ $C = d_0 \frac{\exp(a) + 1}{\exp(b) - 1}$
Central mound	$40 < D < 150$	$h(r) = \begin{cases} (1 - \frac{r}{r_m})h_m - d_0, & r \leq r_m \\ -d_0, & r_m < r \leq r_b \\ C \frac{\exp(br_0) - \exp(b)}{1 + \exp(a + br_0)}, & r_b < r \leq 1 \\ h_r(r^\alpha - 1), & 1 < r \leq 2.5 \end{cases}$	$r_m = 0.293D^{-0.086}$ $r_b = 0.793D^{-0.242}$ $h_m = 0.23 \times 10^{-3}D^{0.64}$ $a = -2.6921$ $b = 6.1678$ $r_0 = \frac{r - r_b}{1 - r_b}$ $C = d_0 \frac{\exp(a) + 1}{\exp(b) - 1}$
Flat-bottomed	$40 < D < 130$	$h(r) = \begin{cases} -d_0, & r \leq r_b \\ C \frac{\exp(br_0) - \exp(b)}{1 + \exp(a + br_0)}, & r_b < r \leq 1 \\ h_r(r^\alpha - 1), & 1 < r \leq 2.5 \end{cases}$	$r_b = 0.091D^{0.208}$ $a = -2.6003$ $b = 5.8783$ $r_0 = \frac{r - r_b}{1 - r_b}$ $C = d_0 \frac{\exp(a) + 1}{\exp(b) - 1}$
Concentric	$40 < D < 160$	$h(r) = \begin{cases} C_1 r^2 + C_2 r - d_0, & r \leq r_i \\ C_3(r - r_i) + h_1, & r_i < r \leq r_o \\ C \frac{\exp(br_0) - \exp(b)}{1 + \exp(a + br_0)}, & r_o < r \leq 1 \\ h_r(r^\alpha - 1), & 1 < r \leq 2.5 \end{cases}$	$C_1 = 0.1920$ $C_2 = 0.0100$ $C_3 = 0.0155D^{0.343}$ $r_i = 0.383D^{0.053}$ $r_o = 0.421D^{0.102}$ $r_0 = \frac{r - r_o}{1 - r_o}$ $a = -1.6536$ $b = 4.7626$ $h_1 = h(r = r_i)$ $h_2 = h(r = r_o)$ $C = -h_2 \frac{\exp(a) + 1}{\exp(b) - 1}$

Note. For all craters, $d_0 = 0.114D^{-0.002}$, $h_r = 0.02513D^{-0.0757}$, and $\alpha = -3.1906$. r is the normalized radial distance, h is the normalized elevation, and D is crater diameter in meters.

larger than 0.6. For the 28 selected impact craters, the normalized residuals between the modeled profile and the observed elevation are smaller than 0.1. Our regressions show a good agreement with previous studies. For example, our depth/diameter ratio of 0.11 is only slightly smaller than those in Daubar et al. (2014) and Sun et al. (2018), Figure S3 in Supporting Information S1. This is mainly because that we used an average crater profile in deriving crater depth whereas Daubar et al. (2014) and Sun et al. (2018) selected the lowest elevations on crater floors.

Using these diameter-dependent morphometric parameters, the topographic profiles of small fresh craters are modeled using a piece-wise function. The selected functions should properly represent crater shape, and also ensure the continuity of the geometric model. For all the four classes of craters, crater wall is modeled by using the sigmoid function (e.g., Gershenfeld & Gershenfeld, 1999) and the elevation beyond crater rim is modeled by using a power law function (Cai & Fa, 2020). The crater floor of a central mound or flat-bottomed crater is flat and hence is modeled as a horizontal line. The uplift of a central mound crater and the inner ring of a concentric crater are straight, and thus they are modeled by using a linear function. The inner pit of a concentric crater is modeled by using a quadratic function. Table 1 shows the mathematical expressions of the constructed crater shape models. Figure 1 also shows four examples of modeled fresh craters with different geometry (red lines). In Table 1, the diameter range for each crater type is obtained based on the selected crater samples, and their upper range values are different. This is consistent with previous studies (Fa et al., 2014; Oberbeck & Quaide, 1967). For example, Fa et al. (2014) found that normal craters are generally smaller than ~100 m in diameter and that most fresh craters with diameters between 120 and ~200 m are concentric. In principle, the upper range of crater

diameter depends on regolith thickness, surface age, and material strength. In our simulation below, we presume our crater profile model for central mound, flat-bottomed, and concentric craters is applicable to a maximum diameter of 180 m.

In this study, the elevation data and the topographic diffusion model are used to quantitatively model the degradation processes of small craters. However, only a small fraction of the lunar surface is covered with meter-scale NAC DTMs (see Figure 1 in Cai & Fa, 2020). In contrast, NAC optical images cover almost the entire lunar surface (Robinson et al., 2010), and hence are a good choice for degradation state identification and regolith thickness estimation. We noticed that crater diameters measured in topography data might be different from that measured in optical images. By comparing the measured diameters of the 28 selected fresh craters in LROC NAC optical images and DTMs, we found that the relative difference in diameter is generally less than 5% (Figure S8 in Supporting Information S1). Therefore, we will not consider the diameter difference in the following analysis because its effect on regolith thickness estimate is minor.

3. Crater Degradation Effect on Regolith Thickness Estimation

In most previous studies (e.g., Fassett & Thomson, 2014; Soderblom, 1970; Xie et al., 2017), crater degradation is hypothesized as a diffusional process mainly caused by the cumulative effect of subsequent small impacts. With the topographic profile model in Section 2, the degradation process of a small crater can be modeled by resolving the standard diffusion equation analytically (Xie et al., 2017). In this model, the degradation state of a crater is completely controlled by the diffusion state κt (or diffusion age, unit: m^2), where κ is the topographic diffusivity and t is time. By studying 800 m to 5 km diameter craters on the lunar maria, Fassett and Thomson (2014) found that κ varies with time and that its mean value over the past 3 Gyr is $5.5 \text{ m}^2/\text{Myr}$.

As an example, we first show the degradation processes of four fresh craters with an initial diameter of 80 m (Figure S9 in Supporting Information S1). The results demonstrate obviously that as a crater degrades, its diameter increases and its morphology changes. A normal crater does not change its morphologic type, and a flat-bottomed or a concentric crater degrades directly into a normal one. A central mound crater first degrades into a flat-bottomed one, and then becomes a normal crater. The results also show that, except for normal craters, a fresh crater 80 m in diameter would change its morphology type quickly within a short time period (e.g., $\kappa t < 10 \text{ m}^2$). According to the topographic profile and surface slope, we set the criteria for crater morphology change identification: (a) a normal crater becomes undetectable when its depth/diameter ratio is smaller than 0.02 (Basilevsky et al., 2014); (b) a central mound crater transforms into a flat-bottomed one when its mound disappears; (c) a flat-bottomed or a concentric crater degrades into a normal one when the slope everywhere within the rim decreases monotonously with time.

Because the morphology of small craters is scale-dependent, the change in diameter and morphology of a crater during its degradation process depends on its initial diameter as well. We further performed extensive simulations for the degradation processes of the four types of craters with diameters ranging from 40 to 180 m (For normal craters, the upper diameter is set to 100 m). Figure 2 shows the evolution path of crater diameter (black line) and morphology type (background color) as a function of diffusion state (κt) and initial diameter. The geological age is calculated by using an average diffusivity of $5.5 \text{ m}^2/\text{Myr}$ (Fassett & Thomson, 2014). These results confirm the morphology change path induced from the above simulations with an initial diameter of 80 m (Figure S9 in Supporting Information S1). Compared with larger ones, the morphology change of smaller craters occurs at a smaller diffusion age. In addition, the results show that a small crater with diameter less than 180 m would disappear within 200 Myr, that is, its lifetime (or survival time) is 200 Myr. From Figure 2, the degradation effect on crater diameter and morphology, and regolith thickness estimation can be deduced (Figures S10 and S11 in Supporting Information S1):

1. For a normal crater (diameter range: 40–100 m), the rim crest diameter (that is determined from simulated elevation data) increases approximately 50% upon its disappearance with an age smaller than 60 Myr. If crater degradation effect is not considered, the lower limit of regolith thickness estimated from a normal crater will be enlarged by a factor of $\sim 50\%$.

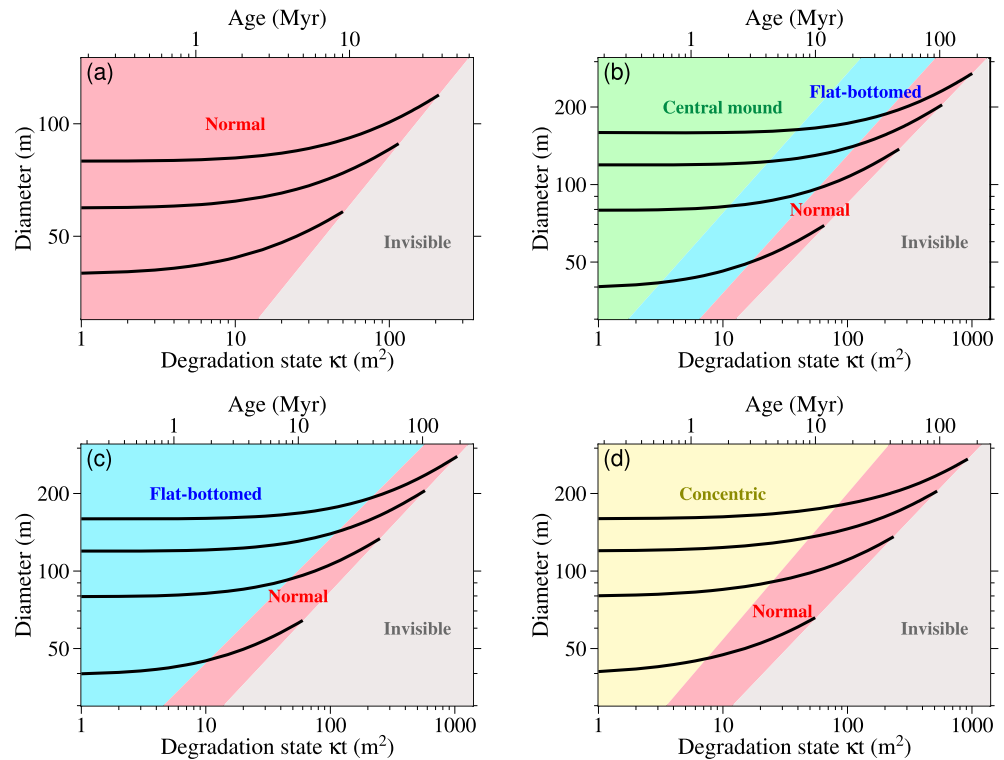


Figure 2. The changes in diameter and morphology as a function of diffusion state (κt) and initial diameter for small craters with different morphology: (a) Normal, (b) Central mound, (c) Flat-bottomed, and (d) Concentric. The black curve represents crater diameter, and the background color represents morphology: red for normal, green for central mound, blue for flat-bottomed, light yellow for concentric, and gray for invisible. The reference geological age is calculated with an average diffusivity of $\kappa = 5.5 \text{ m}^2/\text{Myr}$ (Fassett & Thomson, 2014), and size dependent diffusivity is not considered here.

2. A central mound crater (diameter range: 40–180 m) degrades into a flat-bottomed one at an age no longer than 20 Myr, and its diameter increases by a factor of $\sim 5\%$. Therefore, any small central mound craters on the Moon can be considered as fresh, and the degradation effect on the estimated regolith thickness can be negligible.
3. A flat-bottomed crater (diameter range: 40–180 m; including those evolved from central mound craters) degrades into a normal crater no longer than 100 Myr, upon which its diameter increases $\sim 20\%$. The estimated regolith thickness is changed from $D/9 < d < D/4$ to $d > D/4$. Upon disappearance, the diameter of a flat-bottomed crater would increase by a factor of $\sim 70\%$.
4. A concentric crater (diameter range: 40–180 m) degrades into a normal one no longer than 40 Myr, and the increase in diameter is $\sim 12\%$. As a result, the regolith thickness estimation changes from $d < D/9$ to $d > D/4$. The diameter of a concentric crater increases by a factor of $\sim 70\%$ before it disappears.

In summary, as a small crater degrades, its diameter increases and its morphologic type changes. As a result, when estimating regolith thickness using small crater morphology method, the estimate would be biased to an incorrect value. For this reason, degradation effect should be considered when using this method. Previous studies also show that topographic diffusivity is size-dependent and decreases with crater diameter (Minton et al., 2019; Xie et al., 2017). If size-dependent diffusivity in Xie et al. (2017) is considered, the estimated lifetime of small fresh craters could be about 6 times larger than the results above. This will enlarge the dates for the transformation degradation states by a factor of 6–12 times (see Table S1 in Supporting Information S1). Nevertheless, as the cumulative effect of crater degradation (i.e., diffusion state) is the most important concern in our study, this would not affect the conclusion of the degradation effect on crater diameter, morphology, and regolith thickness estimation.

4. An Revised Method for Regolith Thickness Estimation and Its Applications

Since topographic degradation can change crater diameter and morphology, its effect should be considered when estimating regolith thickness using small crater morphology method. In this section, we propose a revised small crater morphology method for regolith thickness estimation based on crater degradation modeling and spatial correlation of small craters, and we then apply it to the Apollo 11 and 14 landing sites.

4.1. The Revised Small Crater Morphology Method

For regolith thickness estimation from one crater, if high-resolution topography data (e.g., NAC DTM) are available, the initial diameter and morphology of the crater can be obtained by comparing the modeled and the observed topographic profiles. This can give a more accurate estimate of the regolith thickness around the studied crater. If high-resolution topography data are not available, the diameter, morphology, and degradation state of a crater can be measured and identified in optical images (e.g., NAC images) first. Then, the initial diameter of a crater can be estimated by dividing the measured diameter with an empirical number between 1 and 1.7 depending on the degradation state (see Figure S10 in Supporting Information S1). The initial morphology of a crater can be considered as that of the nearest fresh crater with a similar diameter. This is because that if two craters of similar diameters form on a geological unit with a uniformly distributed regolith thickness, then their morphologic types should be the same. Then, regolith thickness can be estimated based on the initial diameter and morphology of the degraded crater. However, as many factors (e.g., solar incidence angle, resolution, and investigator bias) could affect the quantification of crater degradation state in optical images, such modification on regolith thickness estimation is not accurate.

For regolith thickness estimation within a geological unit, a statistically significant result can be obtained if the number of small fresh craters (which is proportional to the study area) is sufficient (e.g., Fa et al., 2014). Here, number of craters is considered to be sufficient if their relative distribution versus diameter is smooth without large fluctuations (a good example is the normal craters with diameter smaller than 40 m in Figure 3e). In contrast, if the number of small fresh craters is insufficient, small degraded craters with degradation effect correction should be included as well in order to obtain a reliable thickness estimate. Under the assumption that small craters and regolith thickness are spatially distributed uniformly within the studying region, the degradation effect on regolith thickness estimation can be corrected by using the Monte Carlo method. The counted small craters are first divided into three degradation classes according to their morphologic prominence (e.g., depth/diameter ratio, inner wall slope, rocks): A (fresh), B (moderately degraded), and C (heavily degraded; Basilevsky, 1976). We further assumed that the degradation state of small craters with respect to time and position is evenly distributed. For a moderately degraded crater (class B), its diameter is divided by a uniformly distributed random number between 1 and 1.4, and for a heavily degraded crater (class C), this number is uniformly distributed between 1.4 and 1.6 (Note that the maximum value of 1.7 is not considered here because severely degraded craters are not counted). The initial morphology of a degraded crater is considered to be that of the nearest fresh crater (class A) with a similar diameter. The difference between their diameters is less than the uncertainty in crater diameter measurement, which is dependent on the spatial resolution of the optical images. By performing the Monte Carlo based correction for a number of realizations, a mean cumulative distribution of regolith thickness can be obtained. When the number of realizations is large enough (e.g., >100), the mean cumulative distribution of regolith thickness reaches stable and does not change with realization number.

4.2. Applications to the Apollo 11 and 14 Landing Sites

The Apollo 11 landing site is located in the south of Mare Tranquillitatis (Figure 3a). A recent detailed geological study based on multispectrum, topography and albedo shows that the landing region is relatively uniform (Iqbal et al., 2019; see also Text S1 in Supporting Information S1). Observations from the in situ passive seismic experiment (PSE) suggested a regolith thickness of 4.4 ± 1.0 m (Nakamura et al., 1975). Di et al. (2016) investigated the regolith thickness at the Apollo landing sites using 3-D morphology method (elevation different between crater floor and background region, and traditional crater morphology method) with a limited number of craters. They found that the regolith thickness at the Apollo 11 landing site is 4.3 m from elevation measurement and 3.3 m by using the traditional morphology method. In addition, meter-scale NAC optical images and DTM are available in

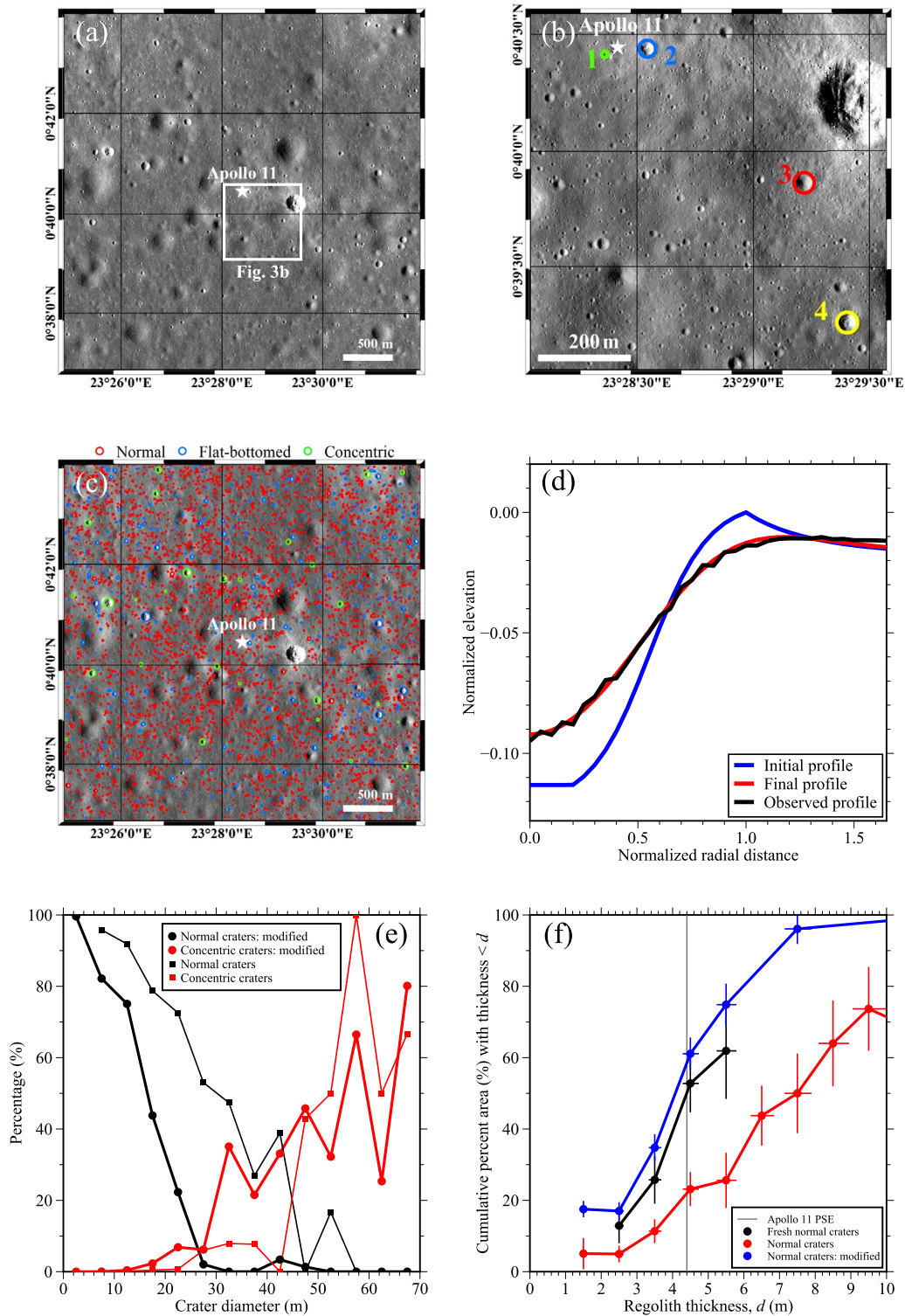


Figure 3. (a) The Lunar Reconnaissance Orbiter Camera Narrow Angle Camera (LROC NAC) images (M135039651RE and M135039651LE) at the Apollo 11 landing site. (b) Four selected craters. (c) All the counted 3,738 small craters. (d) The simulated and observed radial topographic profiles for Crater 3. (e) Relative distribution of normal and concentric craters with (thick lines) and without (thin lines) degradation effect correction. (f) Cumulative distributions of the regolith thickness estimated from fresh normal craters (black), all normal craters (red), and normal craters with considering the degradation effect (blue), where the gray line shows the estimate from the passive seismic experiment.

the landing region. All these make the Apollo 11 landing site an ideal region to validate our revised method for regolith thickness estimation.

We first applied the revised method to individual small craters (Figure 3b). Crater 1 is a fresh normal crater 15 m in diameter. This directly gives a lower limit of 3.75 m for the regolith thickness, which is consistent with the PSE estimation. Crater 2 is a slightly degraded flat-bottomed crater with a diameter of 36 m, and this yields a regolith thickness range between 4.0 and 9.0 m. If the diameter is divided by 1.2, the initial diameter would be 30 m, and the regolith thickness would be between 3.3 and 7.5 m. Crater 3 is a slightly degraded normal crater 44 m in diameter. This crater yields a lower limit of 11 m for the regolith thickness, which is much larger than the PSE estimate. For this crater, we performed a numerical simulation for its degradation process and compared the degraded profile with the observed topographic profile (Figure 3d). The best fit result shows that upon its formation, this is a flat-bottomed crater with a diameter of 43 m. The estimated initial morphology of this crater is the same as crater 4, a fresh flat-bottomed crater 44.6 m in diameter. If initial diameter and morphology of crater 3 are used, the regolith thickness is estimated to be between 4.8 and 10.8 m, which is consistent with the PSE estimate if the 1.0 m uncertainty is considered.

The cumulative distribution of regolith thickness at the Apollo 11 landing region is estimated by using our revised method as well. In the landing region 3.8 km across, we counted 3,738 small impact craters with diameters between 5.6 and 99.1 m, and we also identified their morphologic type and degradation state (Figure 3c and Figure S13 in Supporting Information S1). In total, there are 777 fresh (class A), 1,280 moderately degraded (class B), 1,681 heavily degraded (class C) craters. In terms of morphology, there are 3,301 normal, 407 flat-bottomed, and 30 concentric craters. Figure 3e shows the relative distribution of normal and concentric craters without and with correcting crater degradation effect. As can be seen, our revised method leads to a significant reduction in the proportion of normal craters and an increase in relative number of concentric craters as crater diameter becomes larger than 30 m. As the number of concentric craters is small, only normal craters are used here to obtain a statistically significant result. From Figure 3f, the median value of regolith thickness estimated from fresh normal craters is 4.4 m, which is consistent with PSE estimate. If degradation effect is not corrected, cumulative distribution of regolith thickness is biased to a larger value, and the median value is 7.6 m. When crater degradation effect is corrected, the cumulative distribution is moved leftwards with a smaller regolith thickness, and the median regolith thickness is 4.1 m. This corrected result is very close to the estimate from fresh craters only and the in situ PSE observations, suggesting that our revised method is effective. Our result matches well with the 4.3 m thickness measured from elevation data in Di et al. (2016), but is better than their crater morphology result (3.3 m) because we used a large number of craters.

We further applied the revised method to the Apollo 14 landing site (Text S2; Figures S14 and S15 in Supporting Information S1). The Apollo 14 landing site is located in the highland, which differs from the mare in the Apollo 11 landing region. Target property could affect the morphology of small craters forming in regolith and diffusivity. However, we did not find any noticeable difference in crater morphology between maria and highlands (both in this study and our previous study Figure A1, Cai & Fa, 2020). In addition, the diffusivities of the maria and highlands are almost the same (Du et al., 2019). Therefore, we use the same crater profile model and diffusivity for both the Apollo 14 and 11 landing sites. A degraded normal crater with a diameter of 67.3 m gives a lower limit of 16.8 m for the regolith thickness, much larger than the active seismic experiment (ASE) result of 8.5 ± 2.0 m (Nakamura et al., 1975). Topographic degradation modeling result shows that upon its formation, this crater was a flat-bottomed crater with a diameter of 60 m. Based on this, the regolith thickness is revised to be between 9 and 15 m, consistent with the ASE observations. We counted 2,514 small craters over the Apollo 14 landing region 4×9 km across, including 495 fresh (class A), 833 moderately degraded (class B), and 1,186 heavily degraded (class C) craters (Figures S14b and S16 in Supporting Information S1). Estimation from all the 2,514 craters yields an unreasonable result, that is, the cumulative value of regolith thickness fluctuates around $\sim 20\%$ when regolith is thicker than 10 m (Figure S14f in Supporting Information S1). When the degradation effect is corrected, the cumulative distribution is very similar to that from fresh craters only, and the median regolith thickness is 7 m, which is consistent with the ASE result. Again, these results suggest that the revised method is effective in correcting the degradation effect on regolith thickness estimation.

We noticed that, at both the Apollo 11 and 14 landing sites, our revised method yields a similar, but slightly smaller cumulative distribution of regolith thickness than that derived from fresh craters only. There are two possible reasons. First, the correction number for crater diameter is considered to be evenly distributed, which

does not properly consider the degradation rate with respect to time. A crater degrades faster when it is fresh, but slower when it ages as surface slopes become less steep. Second, the estimated regolith thickness based on all the craters after degradation effect correction reflects the regolith thickness when these degraded craters were initially formed as fresh craters. Estimate from fresh craters only is the present-day regolith thickness. As regolith thickness generally increases with time, the result from degraded craters should be smaller than the estimate from fresh craters. Regolith growth may lead to an incorrect assumption on the initial morphology of small craters. However, as regolith growth is relatively slow during the past 0.15 Gyr (median thickness < 0.2 m; Xie et al., 2021), the difference between estimations from fresh and all the craters is minor, as indicated by the results at the Apollo 11 and 14 landing sites. After 0.15 Gyr degradation, a 70 m diameter crater possesses a depth/diameter ratio < 0.02 (Xie et al., 2017) and becomes invisible. On the other hand, analyzing regolith thicknesses estimated from degraded and fresh craters over a geologic unit might provide a way to study lunar regolith growth rate. We also noticed that the proportion of class A craters compared to class B and C in our study is much higher than that in Basilevsky (1976). Several potential factors could explain this discrepancy, such as local geology of the study regions (age, regolith thickness, and material strength), diameter range of the investigated craters, and investigator bias.

5. Conclusions

In this study, we constructed a topographic profile model for small craters (< 180 m in diameter) with normal, central mound, flat-bottomed, and concentric geometry, and then simulated their degradation processes by using a topographic diffusion model. From the simulations, we quantitatively studied the evolution of crater diameter and morphology, and then investigated the topographic degradation effect on lunar regolith thickness estimation using the small crater morphology method. The results show that topographic degradation can enlarge the diameter of a crater and change its morphology within a short time period, that is, less than 200 Myr. Thus, crater degradation effect should be considered when estimating lunar regolith thickness using small craters. High-resolution (i.e., meter scale) topography data can be used in modeling the degradation process of a small crater in order to obtain a more accurate regolith thickness. For a region of interest, if the number of fresh craters is sufficient, then it is better to use only fresh craters for regolith thickness estimation. Otherwise, if the number of fresh craters is not sufficient, degraded craters should be included in order to obtain a statistically significant estimate of regolith thickness. In this case, the diameter and morphology of the degraded craters can be empirically corrected via the Monte Carlo method based on topographic diffusion modeling and the spatial correlation of small craters.

Applications of the revised method to the Apollo 11 and 14 landing sites yield consistent results as compared to the in situ seismic experiment measurements and those from fresh craters only, suggesting the effectiveness of the revised method. The revised small crater morphology method can be applied to lunar regolith thickness estimation by using high-resolution optical images from recent missions. In addition, comparing regolith thicknesses estimated from fresh and degraded craters might provide a way to study regolith growth rate. All these can provide valuable information for understanding the formation and evolution of lunar regolith and the impact flux in the inner solar system.

Data Availability Statement

The LROC NAC optical images and DTMs are archived at Arizona State University (http://wms.lroc.asu.edu/lroc/rdr_product_select), all the NAC DTMs can be searched by setting “RDR Prefix” to “NAC_DTM”), and Kaguya MI images are available at JAXA (<https://darts.isas.jaxa.jp/planet>). The counted craters and the derived data in this paper are available at Yang et al. (2021).

Acknowledgments

W. Fa conceived the project, led and participated in all aspects of the analysis, and wrote the manuscript. X. Yang constructed the topographic profile model, simulated the crater degradation, proposed the revised method, and drafted an early version of the manuscript. J. Du participated in crater profile model construction, M. Xie helped in topographic degradation simulation, and T. Liu counted the craters at the Apollo 11 and 14 landing sites. All the authors discussed and provided significant comments on the manuscript.

The authors thank two anonymous reviewers for their constructive and helpful comments. The authors gratefully acknowledge NASA PDS Geosciences Node for providing LROC NACs and NAC DTMs data, and JAXA for providing Kaguya MI images. This work was supported partly by the B-type Strategic Priority Program of the Chinese Academy of Sciences (XDB41000000), the National Key Research and Development (2019YFE0123300), and the National Natural Science Foundation of China (12173004, 41941002). This is PKU PRSL Contribution 18.

References

- Bart, G. D., Nickerson, R. D., Lawder, M. T., & Melosh, H. (2011). Global survey of lunar regolith depths from LROC images. *Icarus*, 215(2), 485–490. <https://doi.org/10.1016/j.icarus.2011.07.017>
- Basilevsky, A. (1976). On the evolution rate of small lunar craters. *Lunar and Planetary Science Conference Proceedings*, 7, 1005–1020.
- Basilevsky, A., Kreslavsky, M., Karachevtseva, I., & Gusakova, E. (2014). Morphometry of small impact craters in the Lunokhod-1 and Lunokhod-2 study areas. *Planetary and Space Science*, 92, 77–87. <https://doi.org/10.1016/j.pss.2013.12.016>
- Cai, Y., & Fa, W. (2020). Meter-scale topographic roughness of the Moon: The effect of small impact craters. *Journal of Geophysical Research: Planets*, 125, e2020JE006429. <https://doi.org/10.1029/2020JE006429>
- Daubar, I. J., Atwood-Stone, C., Byrne, S., McEwen, A. S., & Russell, P. (2014). The morphology of small fresh craters on Mars and the Moon. *Journal of Geophysical Research: Planets*, 119, 2620–2639. <https://doi.org/10.1002/2014JE004671>
- Di, K., Sun, S., Yue, Z., & Liu, B. (2016). Lunar regolith thickness determination from 3D morphology of small fresh craters. *Icarus*, 267, 12–23. <https://doi.org/10.1016/j.icarus.2015.12.013>
- Du, J., Fa, W., Wiczeorek, M. A., Xie, M., Cai, Y., & Zhu, M.-H. (2019). Thickness of lunar mare basalts: New results based on modeling the degradation of partially buried craters. *Journal of Geophysical Research: Planets*, 124, 2430–2459. <https://doi.org/10.1029/2018JE005872>
- Fa, W., Liu, T., Zhu, M.-H., & Haruyama, J. (2014). Regolith thickness over Sinus Iridum: Results from morphology and size-frequency distribution of small impact craters. *Journal of Geophysical Research: Planets*, 119, 1914–1935. <https://doi.org/10.1002/2013JE004604>
- Fa, W., & Wiczeorek, M. A. (2012). Regolith thickness over the lunar nearside: Results from Earth-based 70-cm Arecibo radar observations. *Icarus*, 218(2), 771–787. <https://doi.org/10.1016/j.icarus.2012.01.010>
- Fassett, C. I., & Thomson, B. J. (2014). Crater degradation on the lunar Maria: Topographic diffusion and the rate of erosion on the Moon. *Journal of Geophysical Research: Planets*, 119, 2255–2271. <https://doi.org/10.1002/2014JE004698>
- Gault, D. E., Quaide, W. L., Oberbeck, V. R., & Moore, H. J. (1966). Luna 9 photographs: Evidence for a fragmental surface layer. *Science*, 153(3739), 985–988. <https://doi.org/10.1126/science.153.3739.985>
- Gershenfeld, N. A., & Gershenfeld, N. (1999). *The nature of mathematical modeling*. Cambridge University Press.
- Henriksen, M., Manheim, M., Burns, K., Seymour, P., Speyerer, E., Deran, A., et al. (2017). Extracting accurate and precise topography from LROC Narrow Angle Camera stereo observations. *Icarus*, 283, 122–137. <https://doi.org/10.1016/j.icarus.2016.05.012>
- Iqbal, W., Hiesinger, H., & van der Bogert, C. H. (2019). Geological mapping and chronology of lunar landing sites: Apollo 11. *Icarus*, 333, 528–547. <https://doi.org/10.1016/j.icarus.2019.06.020>
- Mahanti, P., Robinson, M., Thompson, T., & Henriksen, M. (2018). Small lunar craters at the Apollo 16 and 17 landing sites—Morphology and degradation. *Icarus*, 299, 475–501. <https://doi.org/10.1016/j.icarus.2017.08.018>
- McKay, D., Heiken, G., Abhijit, B., Simon, S., Reedy, R., French, B. M., & Papike, J. (1991). The lunar regolith. In G. H. Heiken, D. T. Vaniman, & B. M. French (Eds.), *Lunar source-book: A user's guide to the moon* (pp. 285–356). Cambridge University Press.
- Minton, D. A., Fassett, C. I., Hirabayashi, M., Howl, B. A., & Richardson, J. E. (2019). The equilibrium size-frequency distribution of small craters reveals the effects of distal ejecta on lunar landscape morphology. *Icarus*, 326, 63–87. <https://doi.org/10.1016/j.icarus.2019.02.021>
- Nakamura, Y., Dorman, J., Duennebie, F., Lammlein, D., & Latham, G. (1975). Shallow lunar structure determined from the passive seismic experiment. *The Moon*, 13, 57–66. <https://doi.org/10.1007/BF00567507>
- Oberbeck, V. R., & Quaide, W. L. (1967). Estimated thickness of a fragmental surface layer of Oceanus Procellarum. *Journal of Geophysical Research*, 72(18), 4697–4704. <https://doi.org/10.1029/JZ072i018p04697>
- Quaide, W. L., & Oberbeck, V. R. (1968). Thickness determinations of the lunar surface layer from lunar impact craters. *Journal of Geophysical Research*, 73(16), 5247–5270. <https://doi.org/10.1029/JB073i016p05247>
- Robinson, M. S., Brylow, S. M., Tschimmel, M., Humm, D., Lawrence, S. J., Thomas, P. C., et al. (2010). Lunar Reconnaissance Orbiter Camera (LROC) instrument overview. *Space Science Reviews*, 150, 81–124. <https://doi.org/10.1007/s11214-010-9634-2>
- Soderblom, L. A. (1970). A model for small-impact erosion applied to the lunar surface. *Journal of Geophysical Research*, 75(14), 2655–2661. <https://doi.org/10.1029/JB075i014p02655>
- Stopar, J. D., Robinson, M. S., Barnouin, O. S., McEwen, A. S., Speyerer, E. J., Henriksen, M. R., & Sutton, S. S. (2017). Relative depths of simple craters and the nature of the lunar regolith. *Icarus*, 298, 34–48. <https://doi.org/10.1016/j.icarus.2017.05.022>
- Sun, S., Yue, Z., & Di, K. (2018). Investigation of the depth and diameter relationship of subkilometer-diameter lunar craters. *Icarus*, 309, 61–68. <https://doi.org/10.1016/j.icarus.2018.02.031>
- Wilcox, B. B., Robinson, M. S., Thomas, P. C., & Hawke, B. R. (2005). Constraints on the depth and variability of the lunar regolith. *Meteoritics & Planetary Science*, 40(5), 695–710. <https://doi.org/10.1111/j.1945-5100.2005.tb00974.x>
- Xie, M., Xiao, Z., Xu, L., Fa, W., & Xu, A. (2021). Change in the Earth-Moon impactor population at about 3.5 billion years ago. *Nature Astronomy*, 5(2), 128–133. <https://doi.org/10.1038/s41550-020-01241-8>
- Xie, M., Zhu, M.-H., Xiao, Z., Wu, Y., & Xu, A. (2017). Effect of topography degradation on crater size-frequency distributions: Implications for populations of small craters and age dating. *Geophysical Research Letters*, 44, 10171–10179. <https://doi.org/10.1002/2017GL075298>
- Yang, X., Fa, W., Di, J., Xie, M., & Liu, T. (2021). *Effect of topographic degradation on small lunar craters: Implications for regolith thickness estimation*. Zenodo. <https://doi.org/10.1029/2021gl095537>
- Yue, Z., Di, K., Liu, Z., Michael, G., Jia, M., Xin, X., et al. (2019). Lunar regolith thickness deduced from concentric craters in the CE-5 landing area. *Icarus*, 329, 46–54. <https://doi.org/10.1016/j.icarus.2019.03.032>

References From the Supporting Information

- Lemelin, M., Lucey, P. G., Song, E., & Taylor, G. J. (2015). Lunar central peak mineralogy and iron content using the Kaguya Multiband Imager: Reassessment of the com- positional structure of the lunar crust. *Journal of Geophysical Research: Planets*, 120, 869–887. <https://doi.org/10.1002/2014JE004778>
- Otake, H., Ohtake, M., & Hirata, N. (2012). Lunar iron and titanium abundance algorithms based on SELENE (Kaguya) Multiband Imager data. *The 43rd lunar and planetary science conference* (1659).